Preprint
UCRL-JC-139527

Absorptance Measurements of Optical Coatings—A Round Robin

R. Chow, J.R. Taylor, Z.L. Wu, C.A. Boccara, U. Broulik, M. Commandre, J. DiJon, C. Fleig, A. Giesen, Z.X. Fan, P.K. Kuo, R. Lalezari, K. Moncur, H.J. Obramski, D. Reicher, D. Ristau, P. Roche, B. Steiger, M. Thomsen, and M. von Gunten

This article was submitted to
32nd Annual Symposium on Optical Materials for High Power Lasers,
Boulder, CO, October 16 – 18, 2000

U.S. Department of Energy
Lawrence Livermore National Laboratory

October 26, 2000

Absorptance Measurements of Optical Coatings – A Round Robin

Chow, R.[1], Taylor, J. R.[1], Wu, Z. L.[1], Boccara, C. A.[2], Broulik, U.[3], Commandre, M.[4], DiJon, J.[5], Fleig, C.[6], Giesen, A.[6], Fan, Z. X.[7], Kuo, P. K.[8], Lalezari, R.[9], Moncur, K.[10], Obramski H.-J.[6], Reicher, D.[11], Ristau, D.[12], Roche, P.[4], Steiger, B.[3], Thomsen, M.[10], von Gunten, M.[13]

1. Lawrence Livermore National Laboratory P. O. Box 808 Livermore, CA USA 94551	2. ESPCI/CNRS, Laboratoire d'optique 10 rue Vauquelin 75005 Paris, France
3. HTW Mittweida Technikum Plate 17 FG Physik 09648 Mittweida, Germany	4. Laboratoire d'Optique des Surfaces et des Couches Minces ENSPM Domaine Universitaire de St Jerome 13397 Marseille Cedesc 20, France
5. LETI/CEA – CMO CEA/Grenoble 17 rue des Martyrs 38054 Grenoble Cedex 9, France	6. Institut fur Strahlwerkzeuge Pfaffenwaldring 43 D-70569 Stuttgart, Germany
7. Shanghai Institution of Optics & Fine Mechanics P. O. Box 800-211 Shanghai 201800, P.R. China	8. Wayne State University, Dept. of Physics & Astronomy 666 W. Hancock Detroit, MI USA 48201
9. Research Electro-Optics 1855 South 57th Crt. Boulder, CO 80301 USA	10. Eastern Michigan University, Dept. of Physics & Astronomy 303 Strong Hall Ypsilanti, MI 48197, USA
11. S. Systems Corp., Phillips Lab P. O. Box 9316 Albuquerque, NM 87108, USA	12. Laser Zentrum Hannover e.V. Hollerithallee 8 30419 Hannover, Germany
13. Spectra-Physics Lasers, Inc. 1330 Terra Bella Ave. Mountain View, CA 94043 USA	

Keywords: absorptance, optical coatings, argon ion lasers, near-IR lasers

ABSTRACT

An international round robin study was conducted on the absorption measurement of laser-quality coatings. Sets of optically coated samples were made by a "reactive DC magnetron" sputtering and an ion beam sputtering deposition process. The sample set included a high reflector at 514 nm and a high reflector for the near infrared (1030 to 1318 nm), single layers of silicon dioxide, tantalum pentoxide, and hafnium dioxide. For calibration purposes, a sample metalized with hafnium and an uncoated, superpolished fused silica substrate were also included. The set was sent to laboratory groups for absorptance measurement of these coatings. Whenever possible, each group was to measure a common, central area and another area specifically assigned to the respective group. Specific test protocols were also suggested in regards to the laser exposure time, power density, and surface preparation.

1. INTRODUCTION

High performance optical coatings are used in major laboratory projects and commercial applications. The laser fusion projects, which include collaboration between the national laboratories of France and United States, require optics with coatings that survive high-peak power laser fluences. The semiconductor industry's drive towards ultra-violet wavelengths for sub-micron lithographic patterns places demands on low absorbing materials. Very narrow band filters with low scatter- and

absorptance-induced losses are required for the telecommunication market. There are a variety of methods to measure absorptances.[1-6] New techniques such as the photothermal deformation technique, based on laser pumping and probing, are included with more conventional calorimetry and radiometry techniques.

Invitations to participate in an absorptance round robin were mailed to 18 groups world-wide in January of 1998. A majority of the groups supported the round robin idea. Due to limitations on sample size (for example, small curved surfaces are required for the ring-down technique), the availability of common laser wavelengths, and the availability of test equipment during the measurement period, the number of participants submitting data was 12. The measurements were completed in December of 1999.

A report on the state-of-the-art in coating absorption measurement methods appeared warranted given the growing number of groups with photothermal absorption capabilities and the applications using low absorption coatings. A sample set was created for the rough comparison of absorption techniques. Our objectives were to encourage collaborations in the development of physical methods, procedures, and application for coating absorption measurements; compile absorptances from similar samples for absorptance users; and finally, encourage the development of absorption test equipment to support the laser optics industry for the optimization of coating designs and for quality control in a production setting.

2. EXPERIMENTAL SET-UPS

2.1 Measurement techniques

While details of the experimental methods and apparatus can be found in the literature published by various groups, the principles of all the testing methods are based on detection of laser-induced thermal waves due to optical absorption. When a laser beam (pump beam) irradiates a sample, the absorption of optical energy by the sample causes highly localized heating, which in turn produces various physical responses in the sample as well as in the surrounding media. Table 1 summarizes these absorptance measurement techniques.

Table 1 Summary of absorption measurement techniques used in the round robin. The pump wavelength is at the wavelength of interest.

Technique	Abbreviation	Sensing Method
Mirage	Mirage	Low power laser beam deflected by thermally-induced air density changes
Co-linear	Colinear	Low power laser beam parallel to the pump beam deflected by local differential expansion
Surface Thermal lensing	STL	Low power laser wavefront distortion by local differential expansion
Laser Calorimetry	Calor	Temperature measurement of sample substrate by thermocouples.
Radiometry	Radio	Relative temperature difference produced radiated energy.

Eight groups performed absorption measurements in the visible wavelength regime from 511 to 532 nm. The techniques used by these groups are based on the mirage effect (1 group),[7] collinear photothermal deflection (2 groups),[2,4,7,8] surface thermal lens (3 groups),[5,9,10] laser calorimetry (1 group),[11,12] and radiometry (1 group).[6]

Seven groups performed absorption measurements in the near infrared (nIR) wavelength regime from 1030 to 1318 nm. The techniques used by these groups are based on collinear photothermal deflection (1 group),[2,4,7,8] surface thermal lens (1 group),[5,9,10] and laser calorimetry (5 groups).[11,12]

For the mirage technique, the photothermal signals are detected by employing the physical phenomenon that the refractive index of air is temperature and density dependent. The technique uses a modulated laser beam to generate thermal waves in the sample. If the sample is placed in air, the periodic variation in temperature on the sample surface causes periodic thermal expansion of the air in the vicinity of the heated area and hence changes the refractive index in the optical path of the probe laser beam. The probe laser skims over or bounces off the heated area of the sample surface. This detection scheme is also referred to as transverse photothermal deflection technique. The resulting signal is then a periodic angular deflection of the probe beam, which is detected by a quad-cell detector. The resulting signals are then sent to a lock-in amplifier that selectively amplifies the ac part of the signal.

An alternative way to perform the mirage experiment is to detect the change of refractive index inside the sample using a probe laser beam parallel to the pump beam. This technique is referred to as "co-linear" photothermal deflection technique, despite the angular displacement of the parallel pump and probe beams. The other experimental details of the collinear and the transverse detection schemes are similar.

For the surface thermal lens effect, the experimental arrangement uses a probe laser beam that has a similar or larger beam size on the sample surface than that of the pump beam. Pump laser heating generates a surface thermal deformation, which in turn distorts the wavefront of the reflected probe beam in a way similar to a thermal lens of finite size. The surface thermal lens, as predicted by the diffraction calculation and verified by the experimental observation, can cause either photothermal divergence (defocusing) / photothermal convergence (focusing) or complicated interference fringes, depending on the specific geometry used in the detection scheme. Detection of surface thermal lens signals is very similar to that for the traditional thermal lens effect, details of which can be found elsewhere.

For the laser calorimetry method the measurements have been performed in accordance with the international standard on absorptance measurements ISO 11551.

For the laser radiometry technique, a laser beam is focused onto the surface of an optical sample. Since optical materials have low conductivity, the absorption of the laser beam creates a localized hot spot. The temperature difference between the hot spot and a cooler area away from the laser irradiation is measured remotely with a sensitive infrared thermal camera. Finite element analysis that contains the optical, thermal, and structural properties of the illuminated optic can be used to determine the absorptance required to match the observed temperature difference. Many computer simulations were performed over a wide range of absorptances, laser powers, and laser beam diameters. A simple empirical formulation was generated which allowed a rapid absorptance determination albeit with less accuracy than that available from a full computer simulation.

2.2 Measurement protocol

The test conditions used by each group are listed in Tables 2 and 3. In the test protocol, the following suggestions were made. The first suggestion was that the participants do not clean surface of the samples which would preclude any cleaning artifacts from the absorption measurement. Secondly, we suggested that each group try to measure two areas of the samples according to Fig. 1. Each group was asked to measure a common area at the center of the samples. Then, if possible, each group was asked to measure within an area of each sample that was assigned specifically to them. The center of the sample provided a common test area for every participant, but was susceptible to laser-conditioning. The uniquely assigned areas would be unconditioned. There were free areas on each sample available to optimize the alignment and signal-to-noise ratio. Thirdly, the laser power density was to be < 4 kW/cm^2 to avoid laser damage to the samples and any absorptance non-linearity behavior. Fourth, we suggested that the absorptance measurement be made long (4 minutes) and short (seconds) time durations to ascertain time trends.

Three sample sets were generated and had the coatings deposited in the same coating run. Sample set #1 traveled to all but two groups. Sample set #2 was measured and kept as a back-up in case set #1 was damaged or lost. Sample set #3 consisted of smaller substrates for the calorimetry set-up in the Calor.3 test group.

Table 2 Technique and test parameters for absorption in the visible wavelengths. The numbers after the technique serves to distinguish the different groups that use the same technique. "cw' means continuous wave.

Parameter	Units	Calor.1	Mirage	Colinear.1	Colinear.2	STL.1	Radio	STL.2	STL.3
Test order		3	5	6	7	8	9	11	N/A
Wavelength	nm	532	514	514	514	514	511	514	514
Power	Watt	1	5.8	0.2	0.3	0.23	64	1.4	0.2
Beam Diameter	mm	0.8	0.07	0.22	0.1	0.027	2.13	0.3	0.04
Power density	W/cm^2	199	150710	526	3820	40773	1796	1981	15915
AOI	Degree	2	6	15	30	0	10	0	5
Modulation Frequency	Hz	cw	158	13	27	200	cw	535	12
Sample Set	1 or 2	1	1	1	1	1	1	1	2

Table 3 Technique and test parameters for absorption in the nIR wavelengths. Technique abbreviations are defined in Table 1. The numbers after the technique serves to identify the different groups using the same technique. "cw' means continuous wave, "NR" means not reported, and "N/A" means not applicable.

Parameter	Units	Calor.5	Calor.1	Calor.4	Colinear.2	Calor.2	STL.2	Calor.3
Test order		2	3	4	7	10	11	N/A
Wavelength	nm	1064	1064	1030	1064	1064	1064	1318
Power	Watt	4	9	16	0.3	0.4	1.6	1.4
Beam Diameter	mm	0.05	0.8	1	0.1	1	0.3	1
Power density	W/cm^2	203718	1790	984	3820	51	2264	178
AOI	Degree		2	3	30	NR	0	0
Modulation Frequency	Hz	118	pulsed	cw	27	NR	535	cw
Sample Set	1 or 3	1	1	1	1	1	1	3

2.3 Coated samples

The set of optically coated samples included two high reflectors with a design wavelength of 514 nm and a high reflector for the near infrared (1030 to 1318 nm), single layers of silicon dioxide (silica), tantalum pent-oxide (tantala), and hafnium dioxide (hafnia). The coating samples were made utilizing either one of the following two deposition processes: (1) "reactive DC magnetron" sputtering and (2) ion beam sputtering deposition.

2.3.1 Magnetron sputtered films

The single layer films and high reflectors in the visible and the near infrared were deposited by modulated reactive DC magnetron sputtering. The films were sputtered from pure metal targets in an atmosphere of oxygen and argon. The oxygen reacted with the surface of the metal target to create the oxide. The major difficulty with reactive DC magnetron sputtering was that the build up of oxide on the target surface eventually causes arcing, a direct result from dielectric breakdown of the oxide layer. To prevent this, the voltage applied to the magnetron was modulated with a square wave at a frequency of 17kHz and a duty cycle of 80%. By this method, arcing was eliminated and dense, low scatter films were deposited.

The films were deposited in a cryogenically pumped stainless steel box chamber. The chamber base pressure was $3x10^{-6}$ Torr or less at the start of deposition. The tantala films were deposited with a partial pressure of $2x10^{-4}$ Torr argon and $3x10^{-4}$ Torr oxygen. The magnetron voltage was 710 Volts and the current was 2.7 Amperes. The deposition rate was 0.2 nm/s. The hafnia films were deposited with a partial pressure of $4.7x10^{-4}$ Torr argon and $1.2x10^{-4}$ Torr oxygen. The magnetron voltage was 550 Volts and the current was 1.7 Amperes. The deposition rate was 0.1 nm/s. The silica films were deposited with a partial pressure of $1.5x10^{-4}$ Torr argon and $1.5x10^{-4}$ Torr oxygen. The magnetron voltage was 680 Volts and the current was 2.5 Amperes. The deposition rate was 0.2 nm/s.

The high reflector at 514nm consisted of a 29-layer stack of alternating quarter wave layers of tantala and silica. The transmittance of the reflector is shown in Fig. 1. The near infrared high reflector consisted of two-quarter wave stacks, one centered at 1070nm and the other at 1300nm. Each stack consisted of 25 alternating quarter wave layers of tantala and silica.A matching layer of silica was inserted between the stacks and the first and last layer of each stack were permutated to suppress ripples in the high reflectance region.

Transmittance scans of the high reflector (HR) with design wavelengths at 514 and in the near-infrared are shown in Figs. 2 and 3, respectively. Transmittance scans of the silicon dioxide, hafnium dioxide, and tantalum pentoxide single layers are shown in Fig. 4.

2.3.2 Ion beam sputtered mirror

The ion beam sputtered HR was produced using a reactive ion beam sputtering process. The mirror design was (HL)^16 H, where H designates tantala and L designates silica. The coating layers were quarter waves at 523 nm to provide for high reflectance at 514 and 532 nm. The mirror center wavelength was measured to be 525 nm. The films were deposited in a 36" cryogenically pumped box chamber. The deposition source was a RF-excited Kaufman ion gun. The sputtering gas was argon. The target materials were high purity fused silica and tantalum. Ionized oxygen was introduced in the chamber during deposition to provide for complete oxidation of the oxide layers. The deposition rate was ~ 0.1 nm/s for both materials. The fully automated deposition system was housed in a class 1000 clean room. Substrates were cleaned, inspected and loaded into coating fixtures in a class 10 clean room.

Table 5: List of coating samples in sets 1, 2, and 3. Coating set 1 is the traveling set for absorption measurements. Coating set 2 is measured only at Wayne State University, and is kept as a back-up to Coating set 1. Coating set 3 were small samples that were used in a calorimetry test technique.

Coating	Coating Abbreviation	Deposition Method	Coating Materials
High reflector for 511-532 nm	HR; IBS	Ion Beam Sputter	Tantala and Silica
High reflector for 511-532 nm	HR; Mag	Magnetron Sputter	Tantala and Silica
High reflector for 1030 – 1318 nm	HR; Mag,nIR	Magnetron Sputter	Tantala and Silica
Silica single layer	Silica	Magnetron Sputter	Silica
Tantala single layer	Tantala	Magnetron Sputter	Tantala
Hafnia single layer	Hafnia	Magnetron Sputter	Hafnia
Hafnium metal single layer	Hf	e-beam	Hafnium
Uncoated fused silica surface	Un-ctd	None	None

3 RESULTS AND DISCUSSION

3.1 Absorptances in the visible wavelength regime

The absorptance in the visible wavelength regime is plotted as a function of the samples tested and the test techniques. In Fig. 5, the absorptance values from the designated technique are plotted for measurements at the common central area of the samples at a relatively short exposure time. In Fig. 6, the absorptance values from the designated techniques are plotted as a function of the assigned areas of the samples, again for a relatively short exposure time. The large spread in absorptance values from the HR:IBS sample is discussed in Sec. 3.3, Absorptance vs. test sequence. For the rest of this section, these values will be ignored.

Some of the other anomalous absorptance values can be explained. The silica absorptance reported by the STL.2 group was taken on the sample after inadvertent contamination. Therefore this silica value was not used for the calculation of the average silica absorptance value. The STL.2 group also noted that the tantala sample appeared contaminated as well, and this may account for its high absorptance in Fig. 6.

These two figures indicate that a mirage technique tends to measure lower absorptance values, and a calorimetry technique tends to measure higher absorptance values. The other techniques measure absorptances that tend to be bracketed within these values. Absorptances from the center area are bracketed within an order of magnitude or less of each other. Assuming that the tantala sample was contaminated, at least in the assigned area, then the absorptance values from the assigned area are also bracketed within an order of magnitude.

The absorptance of the transmissive multi-layered coatings (made by the same deposition process), where the pump wavelength is not equal to the reflective wavelength of the coating, are more absorbing than the reflective coating, where the pump wavelength is equal to the reflecting wavelength. The higher absorptance may be coming from the pump wavelength irradiating the entire stack. In this situation, absorbing sources from underlying layers and the substrate/coating interface contribute to the total absorptance value.

Also for the magnetron sputtered samples, the absorptances of the single layers and uncoated substrates are less than that of the multi-layer stacks per specific technique. One possibility as to why the single layer absorptances are not much lower than

that from the HR:MAG sample is that the interfaces at the coating/substrate and the coating/air may be contributing to the absorptance.

3.2 Absorptances in the nIR wavelength regime

The absorptance in the nIR regime is plotted as a function of the samples tested and the test techniques. In Fig. 7, the absorptance values from the designated technique are plotted as a function of the center area of the samples at relatively short exposure times. In Fig. 8, the absorptance values from the designated techniques are plotted as a function of the assigned areas of the samples, again for relatively short exposure times. The absorptance values from the HR:IBS sample is discussed in Sec. 3.3 on group sequence and will be ignored for the rest of this section.

The tantala single layer sample behaves similarly in the nIR as in the visible regime even though the calorimetry technique dominates at the nIR wavelengths. However, the STL.2 technique is measuring a nIR absorptance about 10x lower than that at the visible regime for the assigned area. Another group reported a high tantala absorptance value. This may be due to non-uniform contamination of the tantala sample.

In general, the absorptances for a given sample measured at the center of the sample have a smaller spread of values than those taken at the assigned areas. The center produce values that are equal to or lower than that at the assigned area. The exception to this trend is the HR:Mag-nIR sample.

The Hf metal sample has higher absorptances than the dielectric coated samples, and at the shorter wavelength, the absorptance increased. This observation is consistent with materials being more absorbing at the shorter wavelengths, and metals being more absorbing than dielectrics.

3.3 Absorptance with wavelength

The absorptances are plotted as a function of pump wavelength in Fig. 9. The trend is that the absorptance measured at the visible wavelength regime is higher than that measured on the same sample at the nIR wavelength regime. This behavior is expected from physical arguments that energetic (short wavelengths) photons excite electrons from the valence band to the impurity sites near or even into the conduction band. [R. M. Rose, L. A. Shepard, and J. Wulff, "The structure and properties of Materials: electronic properties," John Wiley & Sons, NY, 1966.] The absorptances of mirrors designed for the visible appear to increase with wavelength. The trend is observed with the HR:Mag sample from the Colinear.2 and STL.2 testing, and the HR:IBS sample from the Calor.1 testing. The HR:IBS absorptances are not considered in the other cases because of the assumption of contamination (See Sec. 3.4, Absorptance in terms of group sequence). Only the absorptance of the HR:Mag sample by the Calor.1 method is the exception to this mirror trend. One explanation of the trend is that the pump wavelength is sampling more layers of the mirror at the nIR than at the visible wavelengths. So the absorptance is higher because of increase material contributing to the absorptance rather than a degradation of the material.

3.4 Absorptance in terms of group sequence

The absorptances in the visible wavelength regime are plotted as a function of sample and group sequence, where Figs. 10 and 11 are the absorptances from the center and assigned areas of the samples, respectively. There is no reference to test techniques. To be consistent, the data from the short time exposures are used. Generally, the hafnia sample is more absorbing than silica sample, which is more absorbing than tantala sample. Generally, the magnetron-sputtered mirror designed for 514 m, is less absorbing than the HR designed for the nIR. The higher absorptances are likely caused by the pump laser (511, 514, or 532 nm) irradiating more layers in the nIR mirror than in the visible mirror.

Sample absorptances track together except for the relatively minor deviations in the 1st group, where the HR:IBS sample has a higher absorptance than all other samples and the hafnia sample has nearly the same absorptance as the silica sample. The 1st group made the measurements on samples from Set #2. Another relatively minor flip occurs from the 7th group (sample from Set #1), where the tantala sample has a higher absorptance than the silica sample. In the 9th group, the absorptance difference between the silica and tantala samples are minor.

A major change occurs in the 5th group test, where the HR:IBS sample starts to have absorptances greater than 400 ppm. This is on the order of the contaminated silica sample. The previous test was at a high power density. One conjecture was that the center of the sample was damaged. However, Fig. 11 shows that even the assigned areas show a high absorptance level from 5th test onwards. The HR:IBS sample probably was contaminated.

3.4 Absorptance time trends

The time trend plots, Fig. 12, are plotted with normalized absorptances on the same scale. The time trends were part of the experiment because absorptances of some single layers and multi-layers have been reported to depend on irradiation time.13 For silica and tantala single layers the tendency is for the absorptance to either be stable or increase with exposure time. For the hafnia single layer the tendency is for the absorptance to either be stable or decrease with exposure time. For the 514 nm designed mirror samples, there is an effect of irradiation time on absorptance but the trend is ambiguous. For the multi-layered nIR mirror sample, the absorptance tends to either be stable or decreases. If the HR:IBS sample was contaminated, then the absorptance time trends from the Co-linear.1, STL.1, STL.2, and Radio groups may be the absorptance behavior of dirt in the visible wavelength.

Table 6 summarizes the absorptance dependence on exposure time from the above figures. The STL.3 group tested samples from Set #2, although this does not change any of the general observations. All the techniques except for calorimetry have detected changes of absorptance with irradiation time. The hafnia, HR:Mag, and HR:IBS samples are most susceptible to absorptance changes with irradiation time. The changes for the HR:IBS sample may not all be due to the mirror itself since the Mirage and Colinear.1 group measured the HR:IBS sample prior to an assumed contamination event. A complete explanation for the dependence of absorptance on exposure time is difficult because the changes are not always in the same direction, and some groups did not observe changes on some of the samples.

Table 6 Absorptance changes as a function of time when irradiated with laser light. Ch = changes greater than 10%, NCh = changes is less than 10%, NT = sample not tested.

Technique	Silica	Tantala	Hafnia	HR:Mag	HR:IBS	HR:Mag nIR
Colinear.1	NCh	NCh	Ch	Ch	Ch	Ch
STL.1	Ch	NCh	Ch	Ch	Ch	Ch
STL.2	NCh	NCh	Ch	Ch	Ch	NCh
STL.3	Ch	Ch	NCh	Ch	NCh	Ch
Mirage	Ch	Ch	Ch	Ch	Ch	Ch
Radio	NCh	NCh	Ch	Ch	Ch	NT

The sources of absorptance disparities arise from measurement errors (M), absorptance non-linearity in the material (N) [absorptance depends on power density of irradiation], absorptance instability (I) [laser-induced absorptance changes], spatial non-uniformity (S), and the samples becoming contaminated (C). The contributions of these absorptance effects are estimated to be $M < N < I < S < C$. Measurement repeatability is rather good for these techniques as reported by the respective groups. There are test variations in the pump beam itself that may contribute to the absorptance anomalies and hide effects from non-linear absorptance behavior and laser-induced changes, is not observed when one tries to correlate power density with absorptance. The samples were 25 mm in diameter, which should minimize the effects of S. Contamination was one variable that was difficult to control. The testers were not permitted to clean the samples to preclude variabilities due to cleaning.

SUMMARY

Many absorptance trends are identified. Absorptances measurements of the same samples may vary up to 10x from the value averaged from the submitted data. The absorptances of transmitting multi-layers are higher than that from single layer coatings. The absorptances at the common area tend to be slightly lower than that measured at the assigned area or show no significant difference. The absorptance of single layers decreases with increasing wavelength. Absorptance of a mirror increases when the pump laser wavelength deviates from the designed wavelength of the mirror. Finally, laser exposure time has an effect on absorptance although the trend is ambiguous.

For the next absorptance round robin, the following recommendations are listed to assure better test conditions.

In order to compare the measurement techniques at relatively low, medium and high absorptances, an uncoated, super-polished fused silica substrate, a special multi-layered stack, and a metalized sample set would be generated. A multi-layered stack should be designed to have similar E-fields for all of the pump wavelengths.

If a sample set consists of only three samples, then two sample sets may be sent out together. One set may be wiped cleaned, and the other set treated as in this study where no cleaning was allowed. A procedure for cleanliness wiping should be included and if possible, the wipes and solvent would accompany the samples.

A specific and long irradiation time (i.e. 20 minutes) that accommodates all techniques should be suggested. The information regarding time trends may be technique or material induced, but can be studied in separate tests.

There was no clear evidence of laser conditioning at the common area. The protocol to measure common and assigned areas is not necessary. However, the use of assigned areas in this round did allow one group to continue the measurements due to laser damage at the center of the part.

One group performed an inspection of the samples before performing their tests. Their notes were quite useful, and maybe a simple microscopic inspection should be considered as part of the test protocol, at least for the samples that will be cleaned.

Absorptance measurements of transmissive coatings are generally higher. A possible method of quantifying the absorptance at the substrate/coating interface is to measure the absorptance as a function of transmission, where the transmission is determined by the number of layered-pairs.

Absorptances made on thin single layers are not representative of the material. Absorptances of thin materials may have to be performed in pairs stacked together in a quarter-wave high reflector design. For example, given a set of silica/hafnia, silica tantala, silica/alumina ,and silica/titania samples, the relative absorptances of hafnia, tantala, and titania may be tabulated. The table would be analogous to the galvanic potential tables, where the affinity to corrosion is based on a metallic element's electrochemcial potential difference from the other metal in contact and a convenient zero reference potential is chosen. In the above case, the reference would be the oxide silica.

AUSPICES

This work was performed under the auspices of the U.S. Department of Energy by the University of California, Lawrence Livermore National Laboratory under Contract No. W-7405-Eng-48.

REFERENCES

1. P. A. Temple, "Thin film absorptance measurements using laser calorimetry", in Handbook of Optical Constants of Solids, ed. E. D. Palik, Vol. 1, 135, Academic Press, New York, 1985.
2. V. Loriette, J. P. Roger, A. C. Boccarra, Ph. Gleyzes, and J. M. Mackowski, "Probing for low loss materials at 1.064 micron for interferometric gravitational waves detection", Journal De Physique III 4, C7/631-4, 1994.
3. E. Welsch and D. Ristau, "Photothermal measurements on optical thin films", Appl. Opt. 34, 7239-53, 1995.
4. M. Commandre and P. Roche, "Characterization of optical coatings by photothermal deflection", Appl. Opt. 35, 5021-34, 1996.
5. Z. L. Wu, M. Thomsen, P. K. Kuo, Y. S. Lu, C. Stolz, M. Kozlowski, "Photothermla characterization of optical thin film coatings", Opt. Eng. 36, 251-62,1997.
6. V. G. Draggoo, R. G. Morton, R. H. Sawicki, and H. D. Bissinger, "Optical coating absorption measurements for high power laser systems", Proc. SPIE 622, 186-190, 1986.
7. W. B. Jackson, N. M. Amer, A. C. Boccara, and D. Fournier, "Photothermal deflection spectroscopy and detection", Appl. Opt. 20, 1333-44, 1991.
8. R. Chow, J. R. Taylor, Z. L. Wu, R. Krupe, and T. Yang, "Absorptance measurements of transmissive optical components by the surface thermal lensing technique", Proc. SPIE 3244, 376-85, 1998.
9. M. Commandre and E. Pelletier, "Measurement of absorption in TiO_2 film by a collinear photothermal deflection technique", Appl. Opt. 29, 4276-83, 1990.

10. Z. L. Wu, P. K. Kuo, Y. S. Lu, S. T. Gu, and R. Krupe, "Non-destructive evaluation of thin film coatings using a laser-induced surface thermal lensing effect", Thin Solid Films 290-291, 271-7, 1996.
11. For the laser calorimetry method the measurements are performed in accordance with the international standard on absorption measurements ISO 11551.
12. Meja, P.; Broulik, U.; Pfeifer, U.; Steiger, B. Adaptation of the ISO/DIS 11551 to absorptance measurement of low thermal conductors. Proc. SPIE 2966, 96-104, 1997.
13. R. Chow, J. R. Taylor, Z. L. Wu, "Absorptance behavior of optical coatings for high-average-power laser applications", Appl. Opt. 39, 650-8, 2000.

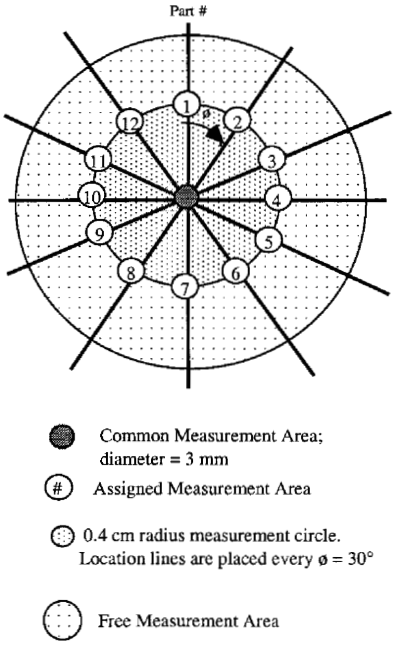

Area Test Group

1 = Wayne State University

2 = HTW Mittweide

3 = Unassigned

4 = Laser Zentrum, Hanover

5 = Unassigned

6 = Institute fur Strahlwerkzeuge

7 = LETI/CEA - CMO

8 = ESPCI/CNRS

9 = Laboratorie d'Optique des Surfaces et des Couches Minces

10 = Eastern Michigan University

11 = Shanghai Institute of Optics and Fine Mechanics

12 = Unassigned

Figure 1 Common and assigned test areas on the absorptance samples.

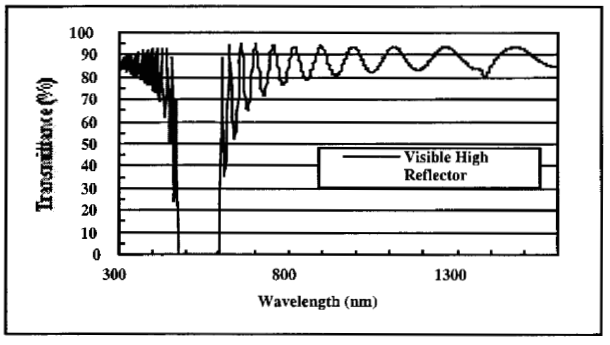

Figure 2 Transmittance on the visible high reflector. The design wavelength was 514 nm, and the multi-layered stack was made of tantala and silica layers.

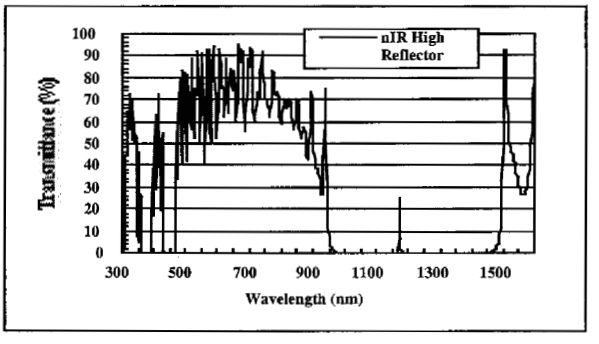

Figure 3 Transmittance of the nIR high reflector. The design reflectance wavelengths were 1064 and 1318 nm, and the multilayered stack was made of tantala and silica layers.

Figure 4 Transmittances of the silicon dioxide, hafnium dioxide, and tantalum pentoxide single layer.

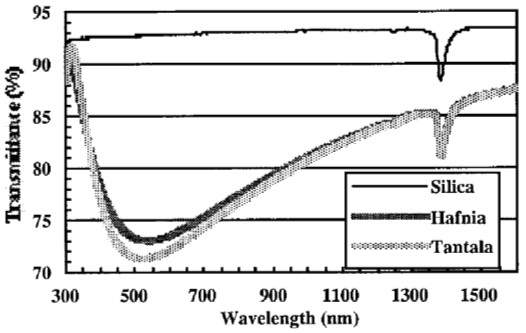

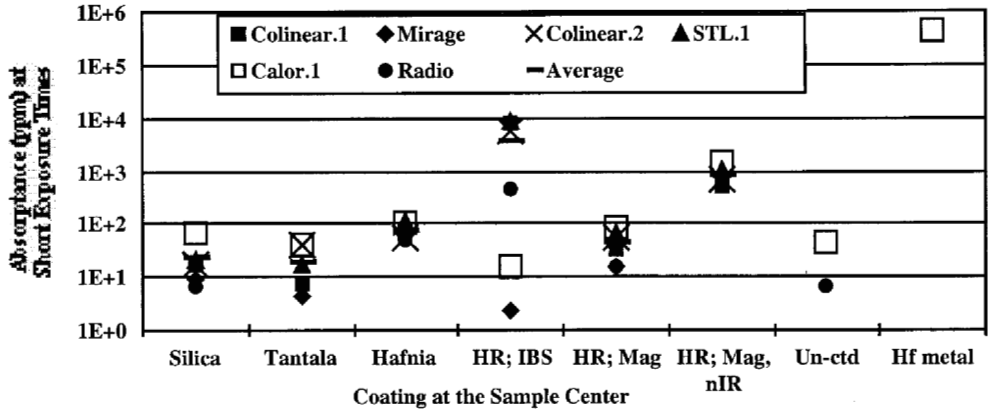

Figure 5 Absorptance in the visible wavelength regime with a relatively short time exposure. The visible wavelength, being either 511, 514, or 532 nm, irradiated the center of sample.

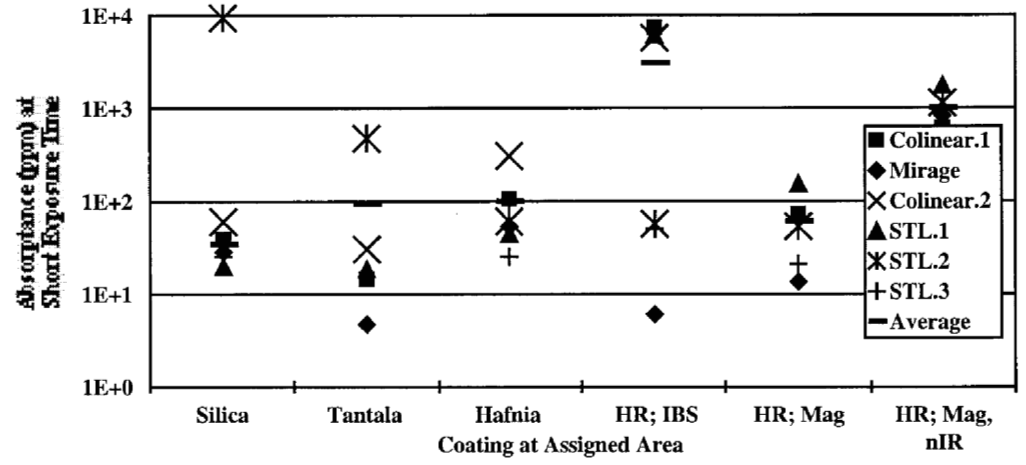

Figure 6 Absorptance in the visible wavelength regime with a relatively short time exposure. The visible wavelength, being either 511, 514, or 532 nm, irradiated the area of the sample assigned to the specified group. The silica average absorptance does not include the data from STL.2 because of unintentional sample contamination. Note that STL.3 measured absorptances on sample set #2, which was coated in the same coating run as sample set #1.

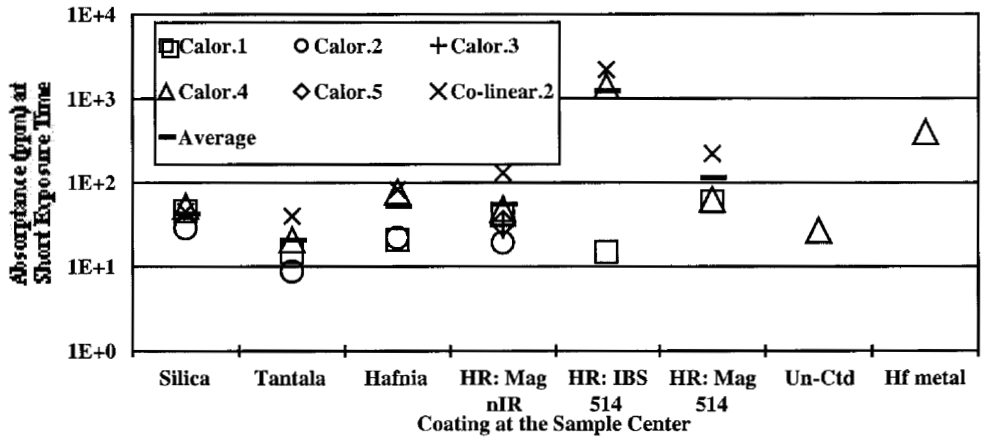

Figure 7	Absorptance in the near infrared wavelength regime with a relatively short time exposure. The nIR wavelength, being either 1030, 1064 or 1318 nm, irradiated the center of sample.

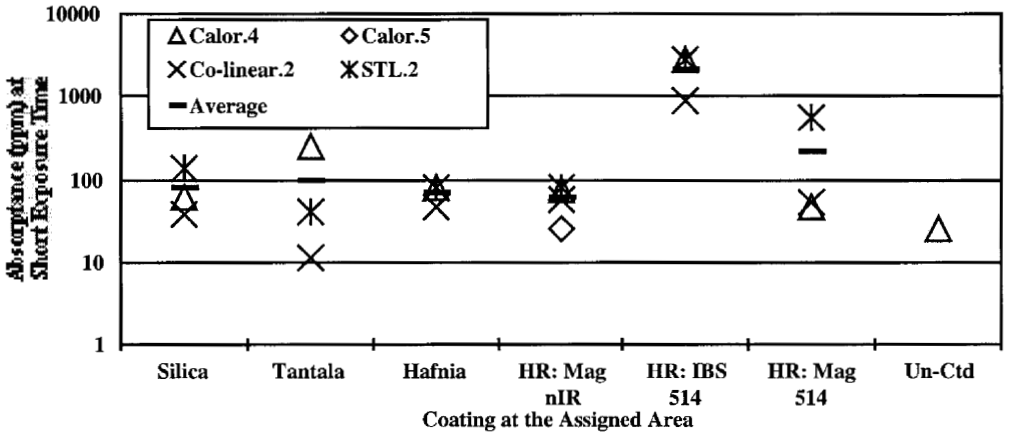

Figure 8	Absorptance in the near infrared wavelength regime with a relatively short time exposure. The nIR wavelength, being either 1030, 1064 or 1318 nm, irradiated the area of the sample assigned to the specified group.

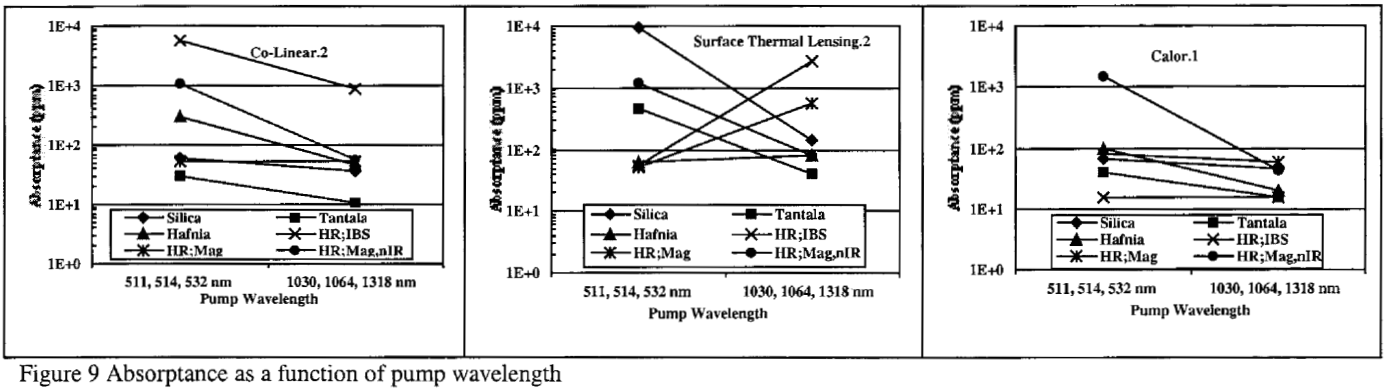

Figure 9 Absorptance as a function of pump wavelength

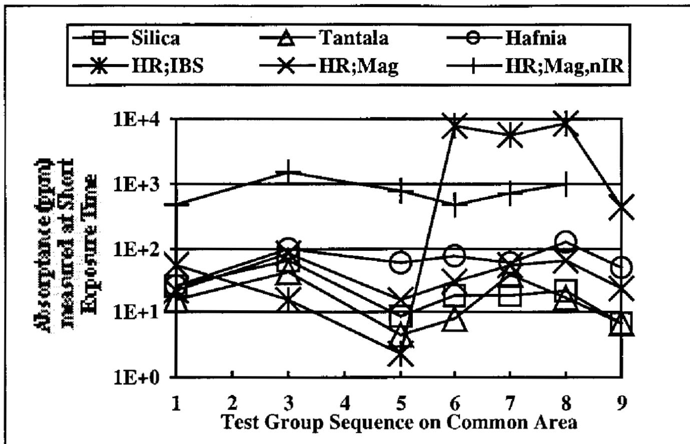

Figure 10 Absorptance (visible, short time exposures) as a function of the test sequence at the center area of the samples.

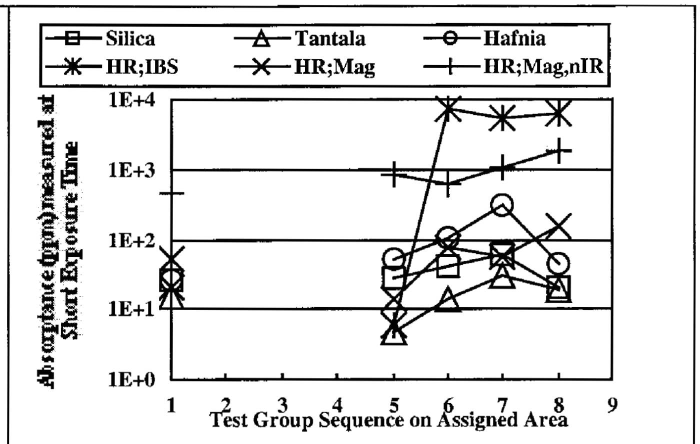

Figure 11. Absorptance (visible, short time exposures) as a function of the test sequence at the assigned area of the samples.

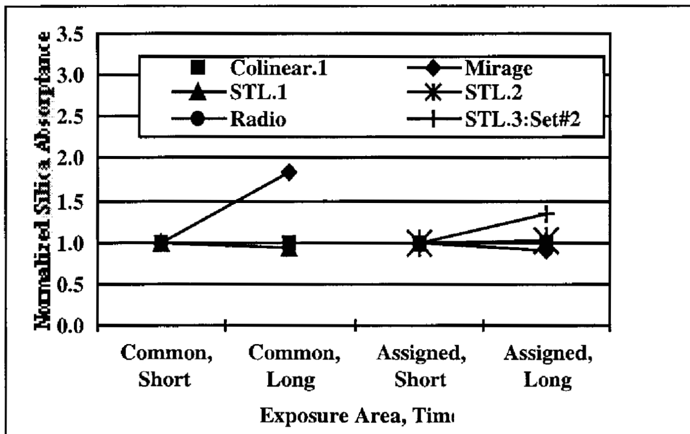

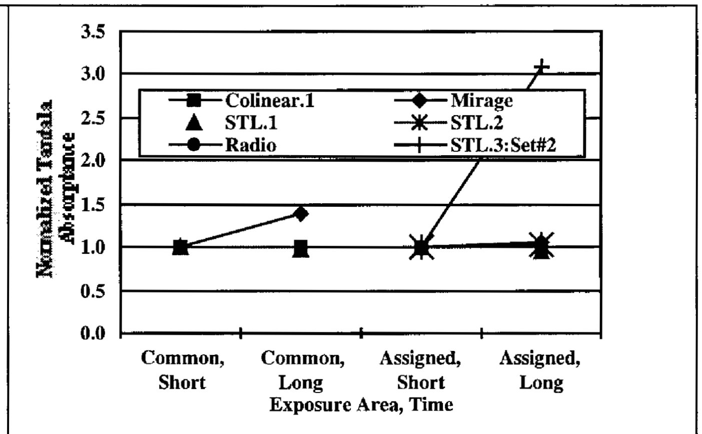

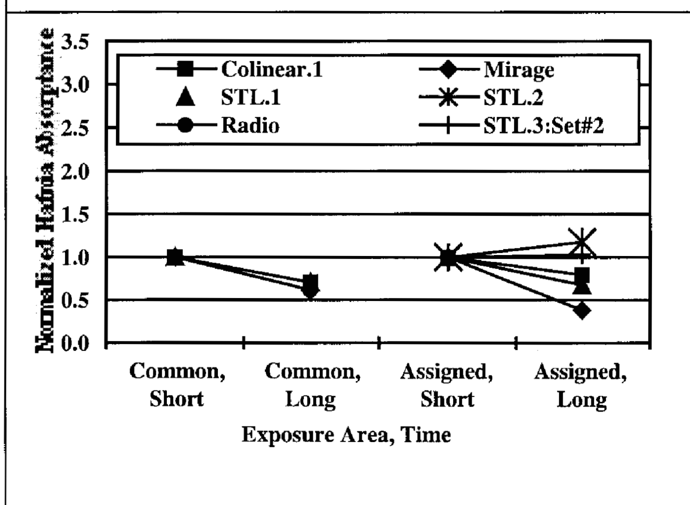

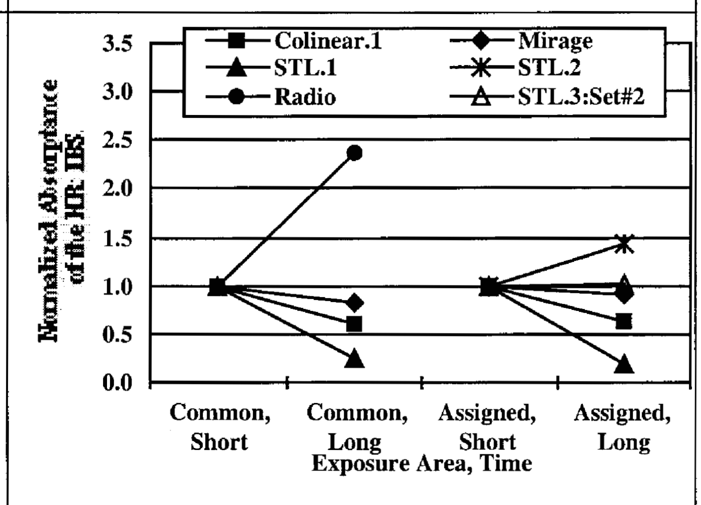

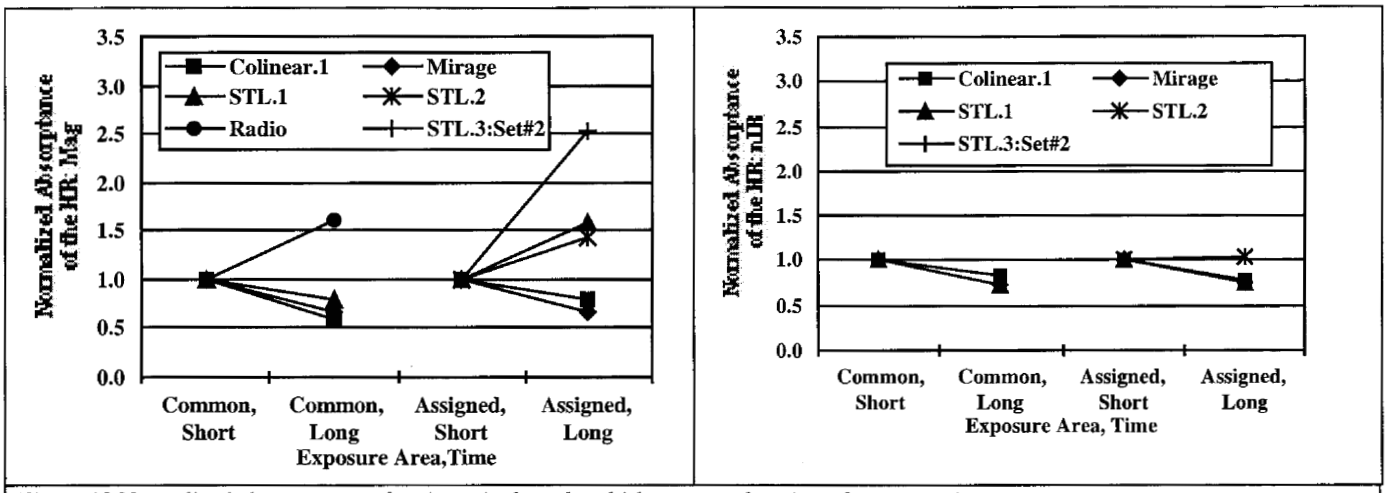

Figure 12 Normalized absorptances of various single and multi-layers as a function of exposure time.